Modeling Neural Crest Induction, Melanocyte Specification, and Disease-Related Pigmentation Defects in hESCs and Patient-Specific iPSCs

Yvonne Mica,[1,2,3] Gabsang Lee,[1,2,4] Stuart M. Chambers,[1,2] Mark J. Tomishima,[1,2] and Lorenz Studer[1,2,*]
[1]The Center for Stem Cell Biology
[2]Developmental Biology Program
[3]Louis V. Gerstner, Jr. Graduate School of Biomedical Sciences
Sloan-Kettering Institute for Cancer Research, 1275 York Avenue, New York, NY 10065, USA
[4]Institute for Cell Engineering, Johns Hopkins University, School of Medicine, Baltimore, MD 21205, USA
*Correspondence: studerl@mskcc.org
http://dx.doi.org/10.1016/j.celrep.2013.03.025

SUMMARY

Melanocytes are pigment-producing cells of neural crest (NC) origin that are responsible for protecting the skin against UV irradiation. Pluripotent stem cell (PSC) technology offers a promising approach for studying human melanocyte development and disease. Here, we report that timed exposure to activators of WNT, BMP, and EDN3 signaling triggers the sequential induction of NC and melanocyte precursor fates under dual-SMAD-inhibition conditions. Using a *SOX10::GFP* human embryonic stem cell (hESC) reporter line, we demonstrate that the temporal onset of WNT activation is particularly critical for human NC induction. Subsequent maturation of hESC-derived melanocytes yields pure populations that match the molecular and functional properties of adult melanocytes. Melanocytes from Hermansky-Pudlak syndrome and Chediak-Higashi syndrome patient-specific induced PSCs (iPSCs) faithfully reproduce the ultrastructural features of disease-associated pigmentation defects. Our data define a highly specific requirement for WNT signaling during NC induction and enable the generation of pure populations of human iPSC-derived melanocytes for faithful modeling of pigmentation disorders.

INTRODUCTION

Epidermal melanocytes are pigment-producing cells found at the basement membrane of the skin, where they establish a photoprotective barrier against UV irradiation. Melanocytes synthesize melanin within specialized lysosome-related structures known as melanosomes, which are subsequently transferred to neighboring keratinocytes, giving the skin its characteristic pigmentation. Although the developmental biology of melanocytes has been well studied in avian and murine models, the pro-

cesses underlying melanocyte development in humans remain poorly understood. The derivation of melanocytes from human embryonic stem cells (hESCs) therefore provides a valuable tool for studying human melanocyte development and modeling disease biology. Previous work on the derivation of melanocytes from murine (Yamane et al., 1999) and human (Fang et al., 2006; Nissan et al., 2011) ESCs relied on stromal coculture or embryoid body formation in combination with conditioned media from a WNT3a-producing stromal cell line to trigger melanocytic differentiation. The lack of a defined culture system has complicated efforts to gain better mechanistic insights into early melanocyte development and maturation.

During development, melanocytes arise from a transient, migratory population of cells that are unique to vertebrates and known as the neural crest (NC). The NC is a multipotent population that exhibits a broad differentiation repertoire with distinct fate potentials along axial levels of origin. Our laboratory previously established a stromal-coculture-based approach for differentiating hESCs into NC with peripheral nervous system (PNS) and mesenchymal competence; however, this population did not efficiently yield melanocyte lineages (Lee et al., 2007). More recently, a neural induction protocol in which hESCs are differentiated under defined dual-SMAD-inhibition (DSi) conditions was found to support low levels of spontaneous NC induction (Chambers et al., 2009) and the emergence of a pigmented cell population. However, most pigmented cells under those conditions exhibit properties of CNS-derived retinal pigment epithelium rather than melanocyte lineage (see Figure S2). Therefore, we sought to establish a novel, defined approach for the derivation of a melanocyte-competent NC population that would enable us to dissect the mechanistic and temporal signaling requirements underlying NC induction, specification along the melanocyte lineage, and melanocyte maturation.

We now report that activation of canonical WNT signaling is sufficient to drive efficient NC specification at the expense of CNS lineages under defined, DSi-based neural induction conditions. We found that a brief pulse of WNT activation is sufficient to induce NC with high efficiency. Remarkably, induction is largely insensitive to pharmacological BMP inhibition and is not dependent on sustained WNT activity. However, derivation of the melanoblast lineage required additional exposure to BMP4
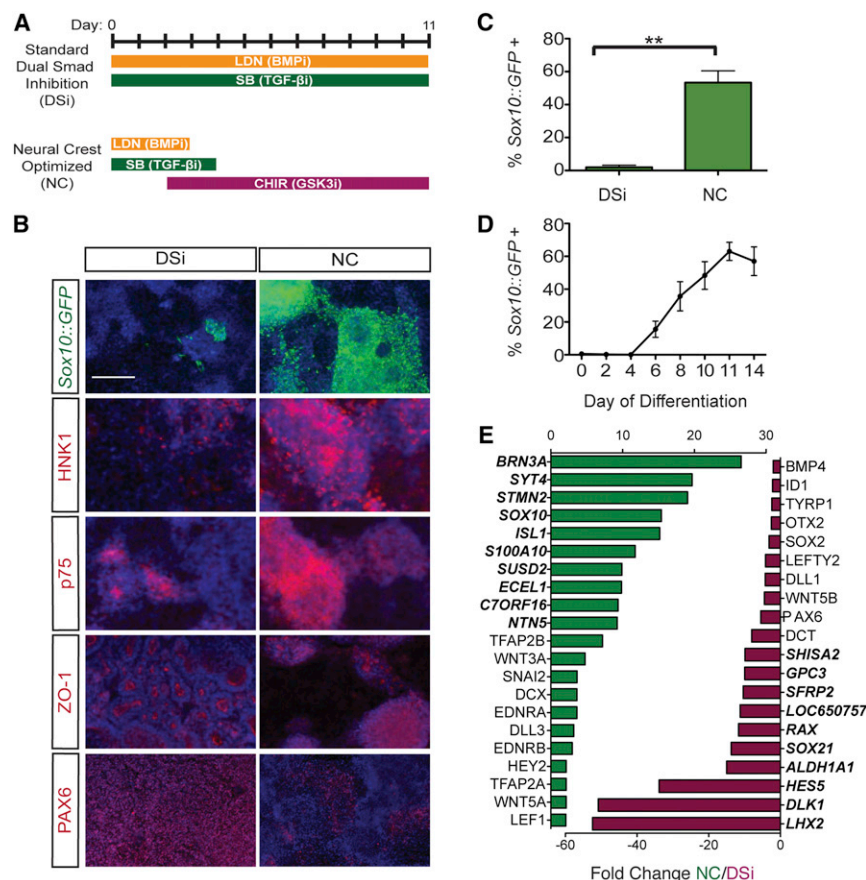
Figure 1. Induction and Isolation of NC from *Sox10::GFP* hESCs Using a Modified DSi Protocol

(A) A DSi protocol can be modified to support highly efficient induction of an NC population by optimizing BMP, TGF-β, and Wnt signaling.

(B) NC conditions support induction of a *Sox10::GFP*-expressing population that coexpresses the NC markers HNK-1 and p75 while downregulating ZO-1- and PAX6-expressing CNS. Scale bars represent 200 μm.

(C) NC-optimized conditions increase the yield of *Sox10::GFP*-positive cells by >20-fold (53% ± 14%, n = 4, p = 0.002) over the DSi condition.

(D) Using FACS analysis, *Sox10::GFP* was first detected at day 6 of NC differentiation and peaked by day 11. *Sox10::GFP* induction efficiency is represented as a percentage of total viable cells.

(E) Significantly upregulated (green) or downregulated (red) genes at day 11 in NC-induced cells compared with DSi cells. Bold genes represent the top ten most differentially regulated genes.

All error bars represent the SEM of at least three independent experiments. **p < 0.01. See also Figures S1 and S2.

SMAD signaling: LDN-193189 (LDN), which inhibits BMP signaling, and SB431542 (SB), which inhibits transforming growth factor β (TGF-β), Activin, and Nodal signaling (Figure 1A). Inhibition of both arms is required to trigger exit from the pluripotent state, prevent trophecto-derm formation, and block the formation of mesendoderm and nonneural ectoderm (Chambers et al., 2009). However, NC specification requires intermediate levels of BMP signaling (Marchant et al., 1998), whereas activation of TGF-β signaling is thought to be required at a later time point to promote the epithelial-to-mesenchymal transition (Xu et al., 2009). To reconcile these opposing requirements, we hypothesized that withdrawal of BMP and TGF-β inhibitors at intermediate time points might allow early inhibition of alternate lineages while facilitating NC specification at later stages by restoring endogenous BMP and TGF-β signaling. Studies in avian models have also established a strong requirement for WNT signaling for early NC specification (García-Castro et al., 2002). We activated Wnt signaling in our system using the potent and cost-effective small molecule CHIR99021 (Chir), which functions as an agonist of WNT signaling by selectively inhibiting glycogen synthase kinase 3β (GSK-3β; Meijer et al., 2004; Ring et al., 2003), although recombinant WNT also efficiently promoted NC induction (Figure S1). The efficiency of NC induction was monitored with a *Sox10::GFP* hESC reporter line (Chambers et al., 2012), which marks early multipotent NC stem cells and specific NC derivatives, including melanocyte progenitors.

We found that inhibition of BMP, TGF-β, and WNT signaling pathways, collectively referred to as the NC-inductive ("NC") condition (Figure 1A), was sufficient to promote robust specification of *Sox10::GFP*-expressing precursors (Figures 1B and 1C).

and EDN3 to induce KIT+ melanocyte-competent NC precursors. We describe defined and scalable culture conditions for the subsequent differentiation, maturation, and long-term maintenance of hESC-derived melanocytes. Finally, we confirm the robustness and utility of our melanocyte differentiation paradigm by modeling pigmentation defects in two independent genetic disorders using patient-specific induced pluripotent stem cells (iPSCs). Differentiation into melanocytes, across all control and disease-specific iPSCs, displayed minimal variability. Furthermore, a direct comparison of disease and control lines identified discrete defects in melanosome loading and transfer by ultrastructural analysis. Our results offer insights into human NC and melanocyte specification, and present a defined and efficient protocol for generating human melanocytes from PSCs that faithfully reproduce patient-specific pigmentation defects.

RESULTS

Derivation of NC from hESCs

To recapitulate the progressive differentiation that occurs during normal development, we established a stepwise differentiation protocol in which human PSCs (hPSCs) are first differentiated to the multipotent NC stage before becoming melanoblast precursors capable of maturing into terminally differentiated melanocytes. In the DSi protocol, hESCs are treated for 11 days with two small molecules that inhibit the separate branches of

Compared with the standard DSi protocol, the NC-optimized condition increased the yield of *Sox10::GFP*-positive cells by >20-fold (53% ± 14%; Figure 1C). Induction of *Sox10::GFP* occurred rapidly, with GFP expression first detectable by flow cytometry at day 6 of differentiation and peaking by day 11 (Figure 1D). The ratio between CNS and NC differentiation was found to be density dependent under DSi conditions, in agreement with a previous study (Chambers et al., 2009), whereas density-dependent differences in yield were less pronounced under NC conditions (Figure S1). Efficient induction of *Sox10::GFP* correlated with an increase in HNK-1 and p75 expression—two markers that were previously found to define hESC-derived NC populations (Lee et al., 2007). However, *Sox10::GFP* did not exclusively colabel with HNK-1 and p75, suggesting that these markers may not represent identical populations of NC (Figure S1). Specifically, the *Sox10::GFP*-positive population contained p75 single-positive cells, whereas the *Sox10::GFP*-negative population also included p75/HNK1 double-positive cells. NC conditions did not support the emergence of ZO-1-expressing neural rosettes or CNS-associated PAX6 expression (Elkabetz et al., 2008; Figure 1B). A comparative gene-expression analysis of day 11 DSi and NC cells further confirmed that NC differentiation conditions favored induction of NC-associated markers, including *SOX10*, *TFAP2A/B*, *SNAI2*, and *EDNRA/B*, as well as genes associated with WNT (*WNT3A* and *LEF1*) and Notch signaling (*DLL3* and *HEY2*; Figure 1E; Table S1), whereas DSi cells expressed high levels of genes associated with CNS (*PAX6* and *HES5*) and forebrain state (*OTX2* and *LHX2*). Fate-specific markers were also induced under both NC and DSi conditions with *BRN3A*, an early marker of sensory neurogenesis that is observed following NC differentiation. Genes associated with pigmentation, such as tyrosinase-related protein 1 (*TYRP1*) and dopachrome tautomerase (*DCT*), were observed under DSi conditions, presumably due to the presence of retinal pigment epithelium cells, which can be expanded under DSi conditions (Figure S2), although DCT is also expressed in the mouse forebrain (Steel et al., 1992). Unlike previously reported NC populations derived from hESCs under stromal coculture conditions (Lee et al., 2007), the NC-derived cells did not exhibit high levels of HOX gene expression, suggesting that these cells correspond to the HOX-negative NC lineage, which was previously shown to be particularly plastic (Creuzet et al., 2005; Le Douarin et al., 2004). However, the A-P axial level, including HOX gene expression, could be manipulated with the use of caudalizing cues such as FGF2 or retinoic acid (RA) treatment (Figure S1).

NC Induction Is Driven by a Narrow Window of GSK-3β Inhibition

To further investigate the individual contributions of the BMP, TGF-β, and GSK-3β inhibitors to NC specification, we performed timed withdrawal experiments during the 11 day differentiation or omitted factors entirely (Figures 2A–2C). Although a brief treatment with LDN was required for *Sox10::GFP* induction, 2–3 days of treatment appeared to be sufficient for optimal NC specification. These findings contrast with a recent report in which treatment with Noggin, another BMP inhibitor used in the original DSi protocol, was found to be dispensable for the

induction of a p75+/HNK1+ NC population (Menendez et al., 2011). We observed similar requirements for TGF-β/Activin inhibition. Conditions in which the inhibitor SB was omitted entirely were not permissive for NC differentiation, whereas withdrawal at any point after day 4 allowed for robust *Sox10::GFP* induction (Figure 2B). Continued treatment with either the BMP or TGF-β inhibitors for the entire 11 days of differentiation did not negatively impact the *Sox10::GFP* yield, suggesting that derepression of endogenous BMP or TGF-β signaling is not essential for triggering NC differentiation (Figures 2A and 2B).

When we investigated the requirements for WNT activation using the small molecule Chir, we observed a narrow window during which Chir treatment was essential for *Sox10::GFP* induction. Although Chir exposure starting at day 2 of the differentiation resulted in optimal *Sox10::GFP* induction, changing the onset of Chir treatment by as little as 2 days resulted in a near-complete loss of *Sox10::GFP* expression (Figure 2C). When we investigated the minimal duration of WNT activity required for *Sox10::GFP* induction, we found that a single day of Chir treatment was sufficient to achieve 70% of the maximal yield (Figure 2D). To test whether a short pulse of Chir treatment could induce a subsequent wave of endogenous WNT signaling, we performed luciferase-based WNT reporter assays. We observed that β catenin levels remained elevated 3 days after a single day pulse of Chir treatment, suggesting that endogenous WNT signaling was indeed triggered by brief Chir exposure (Figure S3). However, blocking endogenous WNT signaling after 1 day of Chir treatment using the axin-stabilizing small molecule XAV-939 (XAV) did not affect the efficiency of NC induction (Figure S3). Our data indicate that WNT signaling is not required beyond a brief inductive pulse to specify NC fate.

We next performed a global gene-expression analysis to determine which transcripts were regulated immediately after Chir exposure (Figures 2E–2H). Within 24 hr of Chir addition, the most upregulated gene was *SP5*, a transcription factor downstream of WNT and beta-catenin signaling that has been implicated in anterior-posterior patterning (Fujimura et al., 2007; Weidinger et al., 2005). Upregulation of *AXIN2* and *WNT1* at 24 hr and 6 days after Chir addition further confirmed that Chir treatment induces endogenous WNT signaling. In contrast, *SIX3*, a negative regulator of WNT signaling that is required for vertebrate forebrain development (Braun et al., 2003; Lagutin et al., 2003; Lavado et al., 2008), and *HESX1* and *SOX3*, two additional forebrain markers, were suppressed following Chir treatment (Figure 2E). By day 6 of the differentiation, the time point when *Sox10::GFP* expression was first observed, induction of various additional NC markers, including *EDNRA*, *SOX10*, *SNAI2*, *TFAP2A/B*, *FOXD3*, *SOX9*, and *PAX3* (Figure 2F), was observed, whereas various CNS and forebrain markers were suppressed (Figure 2F). By days 8 (Figure 2G) and 11 (Figure 2H), more mature, cell-type-specific markers, including *ASCL1*, *EDNRB*, and *OLIG2*, were upregulated. Our global transcriptome profiling data therefore establish a model in which treatment with the GSK-3β inhibitor Chir during the NC protocol first induces a surge of WNT signaling, followed by markers of NC specification and a subsequent neurogenic wave.

We next determined whether the surprisingly narrow window during which WNT signaling drives NC specification reflects a
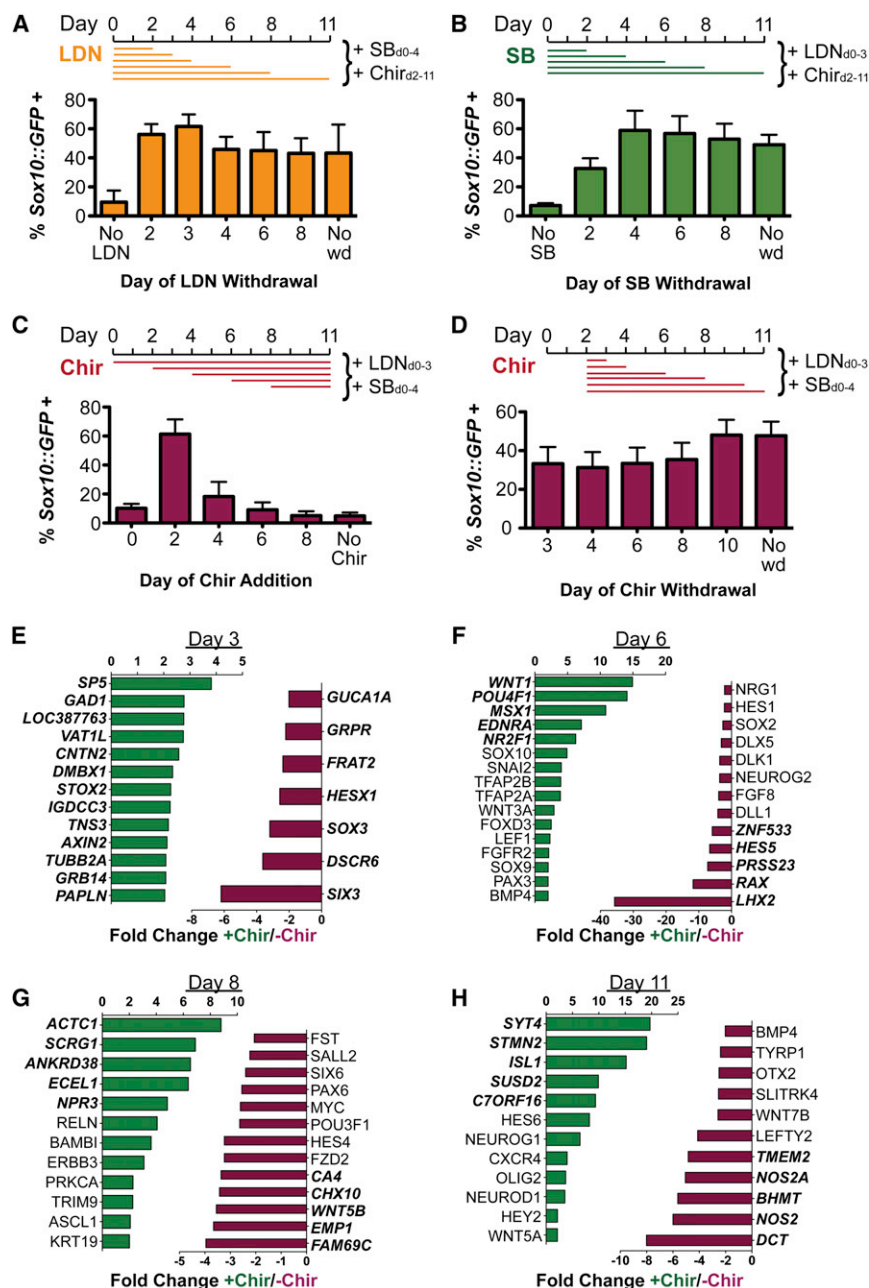
Figure 2. NC Induction Is Driven by a Narrow Window of Wnt Activation

(A and B) BMP inhibitor LDN193189 (LDN) (A) and TGF-β inhibitor SB431542 (SB) (B) were individually withdrawn at various time points within the context of the NC protocol, and induction of *Sox10::GFP* was assessed at day 11 by FACS.

(C and D) Treatment with GSK-3β inhibitor CHIR99021 (Chir) was initiated (C) or withdrawn (D) at various time points, and induction of *Sox10::GFP* was assessed at day 11 by FACS. *Sox10::GFP* induction efficiency is represented as a percentage of total viable cells.

(E–H) The effects of Chir on gene expression at days 3 (E), 6 (F), 8 (G), and 11 (H) were determined by comparative microarray analysis of NC cells derived in the presence (green) or absence (red) of Chir. Bold genes represent the top five most differentially regulated genes.

All error bars represent the SEM of at least three independent experiments. See also Figure S3.

ingly, levels of the negative WNT regulator *SIX3*, which is usually downregulated upon Chir treatment, remained elevated with late Chir treatment. Induction of late WNT-responsive genes was similarly lost (Figure S3). These data indicate that cells lose competency to NC-inductive WNT signals and undergo a default anterior neuroectodermal program.

Lineage Specification and Isolation of NC-Derived Melanoblasts

To confirm the melanocyte competence of our NC-derived cells, we identified a subpopulation of presumptive melanoblasts at day 11 of differentiation based on coexpression of *Sox10::GFP* and microphthalmia-associated transcription factor (MITF; Figure 3A). MITF-positive cells lacking *Sox10::GFP* expression were also observed, which may be due to downregulation of the BAC reporter, as we observed continued SOX10 protein expression by immunofluorescence (see Figure 5E). To prospectively identify and isolate melanoblasts from the heterogeneous population of NC cells, we selected KIT (c-kit) as a putative cell-surface marker of early melanocyte progenitors. KIT was previously identified as uniquely marking the melanocyte-competent subfraction of NC cells (Luo et al., 2003; Reid et al., 1995) and plays an important role in melanocyte migration (Kunisada et al., 1998; Yoshida et al., 1996), proliferation (Kunisada et al., 1998; Yoshida et al., 1996), and maturation (Kunisada et al., 1998). Using fluorescence-activated cell sorting (FACS) analysis, we confirmed that 9% ± 2% of the population at day 11 of differentiation coexpressed *Sox10::GFP* and c-kit, whereas 59% ± 3% expressed only *Sox10::GFP* (Figure 3B).

unique temporal competence of the cells that respond to NC-inductive WNT signaling. Our gene-expression analysis had identified genes induced with 24 hr and 6 days of Chir treatment (Figures 2E and 2F). We asked whether these genes would also be induced when Chir treatment was delayed until day 4 of differentiation, a time point that does not efficiently support NC specification (Figure 2C). We found that many of the genes that were upregulated within 24 hr of Chir treatment, including those known to be direct targets of WNT signaling, were not induced when cells were treated with Chir at day 4 (Figure S3). In fact, upon delayed Chir treatment, many Chir-responsive genes were expressed at levels comparable to DSi conditions. Intrigu-
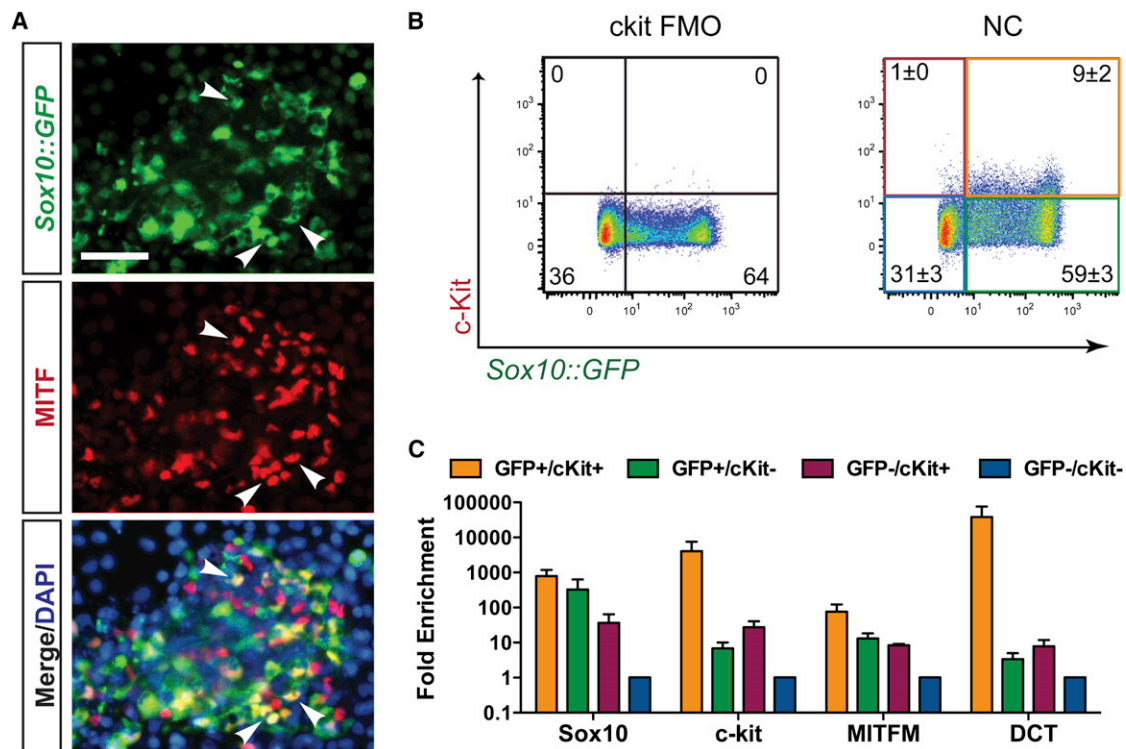
Figure 3. C-kit and Sox10 Expression Can Be Used to Identify and Isolate Melanoblasts
(A) Melanocyte progenitors can be identified in day 11 NC protocol-derived populations by coexpression of *Sox10::GFP* and the melanocyte transcription factor MITF (arrowheads). Scale bar represents 50 μm.
(B) Flow cytometry reveals the presence of a *Sox10::GFP* and c-kit coexpressing population. C-kit "fluorescence minus one" (FMO) was used as a gating control for c-kit staining.
(C) Four-way FACS for *Sox10::GFP* and c-kit reveals an enrichment of the melanocyte markers MITFM and Dct in the SOX10/c-kit double-positive population by quantitative RT-PCR (qRT-PCR).
All error bars represent the SEM of at least three independent experiments. See also Figure S4.

Purified *Sox10::GFP*, c-kit coexpressing (GFP+/cKit+) cells expressed higher levels of the melanocyte markers *MITF-M* and *DCT* when compared with GFP+/cKit− cells (Figure 3C), confirming the utility of KIT and Sox10 coexpression as an appropriate strategy for melanoblast isolation. We performed a candidate screen for factors that increase the percentage of GFP+/cKit+ cells. Contrary to predictions based on literature in other model systems, SCF signaling at this time point did not increase melanoblast numbers; however, we identified BMP and Endothelin 3 (EDN3) as two factors that did enhance melanoblast yield when introduced at day 6 of differentiation (Figure S4). The role of BMP signaling during melanocyte specification has been well established (Nissan et al., 2011; Thomas and Erickson, 2008), and endothelins have been implicated in the maintenance and proliferation of melanocyte precursors (Baynash et al., 1994; Dupin and Le Douarin, 2003; Lahav et al., 1996; Reid et al., 1996). Combined treatment with both BMP4 and EDN3 (hereafter referred to as the "BE" condition) significantly increased the percentage of GFP+/cKit+ cells to 37% ± 3% (Figure 4A). We observed robust expression of *SOX10*, *KIT*, *MITF-M*, and *DCT* within the GFP+/cKit+ population under both NC (Figure 3C) and BE (Figure S5) conditions. However, BE-derived melanoblasts expressed significantly higher

levels of *MITF-M* and *DCT* than the same population derived with the NC protocol (Figure 4B), suggesting that treatment with BMP4 and EDN3 not only enhances melanoblast yield but also further drives their maturation. A comparison of the relative proportions of *Sox10::GFP*- and KIT-expressing populations following NC and BE treatment revealed that BE conditions increased the yield of double-positive melanocyte progenitors, whereas the percentage of *Sox10::GFP* single-positive NC was reduced (Figure 4C). However, the percentage of double-negative cells (GFP−/cKit−) remained unchanged. This change in population makeup could be due to a direct fate switch within the existing NC population. However, we cannot rule out the possibility that increased proliferation of existing melanoblasts or inhibition of nonmelanocyte NC contributes to the BE-mediated increase in melanocyte precursors. Comparative global gene-expression profiling of cell populations derived with the NC and BE protocols confirmed the enhanced expression of various melanocyte-associated markers, including *TYRP1*, *MLANA*, *DCT*, *TYR*, and *SILV*, following treatment with BE (Figures 4D and S5). In contrast, NC-derived populations displayed a gene-expression profile associated with sensory and nociceptor neuron fates (Chambers et al., 2012). BE treatment also induced substantial upregulation of *COL3A1* and *CRYAA*
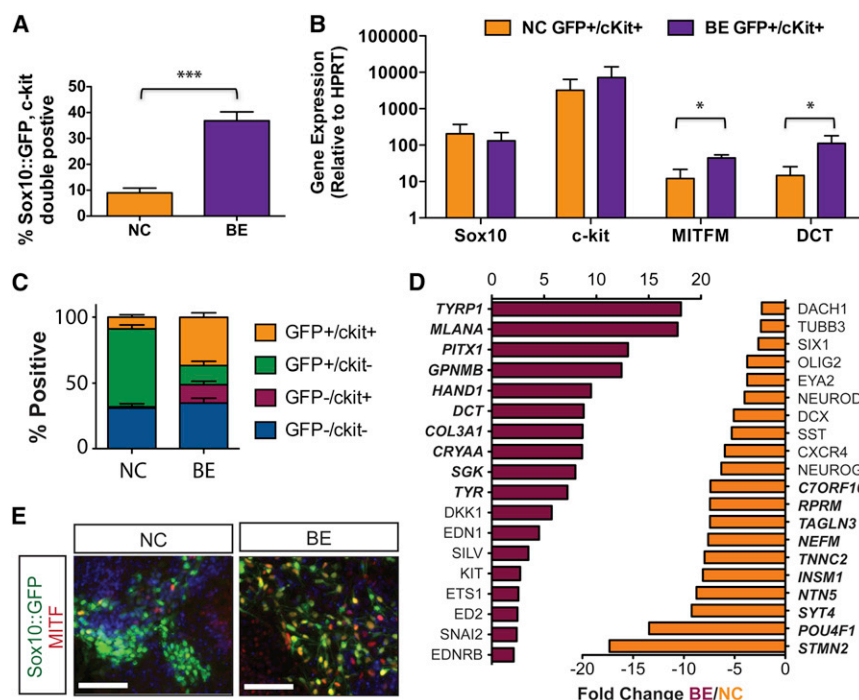
A

% Sox10::GFP, c-kit double postive

50
40
30
20
10

***

NC   BE

B

Gene Expression (Relative to HPRT)

100000
10000
1000
100
10
1

□ NC GFP+/cKit+   ■ BE GFP+/cKit+

*   *

Sox10   c-kit   MITFM   DCT

C

% Positive

100

50

0

NC   BE

■ GFP+/ckit+
■ GFP+/ckit−
■ GFP−/ckit+
■ GFP−/ckit−

D

0   5   10   15   20

TYRP1
MLANA
PITX1
GPNMB
HAND1
DCT
COL3A1
CRYAA
SGK
TYR
DKK1
EDN1
SILV
KIT
ETS1
ED2
SNAI2
EDNRB

−20   −15   −10   −5   0

DACH1
TUBB3
SIX1
OLIG2
EYA2
NEUROD1
DCX
SST
CXCR4
NEUROG1
C7ORF16
RPRM
TAGLN3
NEFM
TNNC2
INSM1
NTN5
SYT4
POU4F1
STMN2

Fold Change BE/NC

E

Sox10::GFP
MITF

NC   BE

Figure 4. Treatment with BMP4 and EDN3 Enhances Melanoblast Specification

(A) Additional treatment with BMP4 and EDN3 (BE) beginning at day 6 significantly enhances the yield of *Sox10::GFP*, c-kit double-positive melanocyte progenitors (n = 4, p = 0.0005).

(B) BE-derived melanocyte progenitors express significantly higher levels of MITF and DCT than NC-derived cells by qRT-PCR (n = 3; p = 0.03 [MITF], p = 0.05 [DCT]).

(C) BE treatment increases the yield of *Sox10::GFP*, c-kit double-positive melanocyte progenitors at the expense of *Sox10::GFP* single-positive NC cells.

(D) Comparative gene-expression analysis identified significantly upregulated (red) and downregulated (orange) genes at day 11 in BE-induced cells compared with NC cells. Bold genes represent the top ten most differentially regulated genes.

(E) BE-derived melanocyte progenitors exhibit spindle-like melanocyte morphology.

Scale bars represent 50 μm. All error bars represent the SEM of at least three independent experiments. *p < 0.05. See also Figure S5.

(Figure 4D). Our group previously observed transient expression of *COL3A1* and several crystallin transcripts in neural rosette-stage cells (Elkabetz et al., 2008). However, future studies are required to address whether *COL3A1* and *CRYAA* are expressed in NC-stage melanocyte precursors or represent contamination with another cell type induced under BE conditions, as those gene expression analyses were performed on unpurified BE bulk populations. BE-derived *Sox10::GFP* cells that coexpressed MITF exhibited an elongated, spindle-like morphology compatible with the appearance of melanocyte progenitors (Figure 4E).

Maturation and Characterization of Melanocytes

Melanoblast progenitors were isolated on day 11 based on *Sox10::GFP* and KIT expression and replated in maturation media (Figure 5A). We next established defined culture conditions for melanocyte maturation. A previous melanocyte differentiation medium was based on the use of conditioned media from a WNT3A-producing murine cell line (Fang et al., 2006). Although we found the same media to be sufficient for maturation of BE-derived melanoblasts to a pigmented, terminally differentiated state (Figure S6), we developed defined maturation conditions using a medium containing SCF, EDN3, FGF2, Chir, cyclic AMP, BMP4, and B27 (Figure S6). Under these conditions, pigmented cells were first observed by bright-field microscopy 6 days after sorting and coexpressed the melanocyte marker MITF (Figure 5B). By day 20 of differentiation, most clusters were pigmented (Figure 5C) and cell pellets became darkly colored by passage 5 (Figure 5D). Extended culture supported the propagation of an essentially pure population of melanocytes expressing typical melanocyte transcription factors, such as MITF and SOX10, and melanosomal markers, such as tyrosi-

nase-related protein 1 (TYRP1) and premelanosome protein (PMEL; Figures 5E and S6). A comparison of gene-expression profiles of mature melanocytes and day 11 melanoblast progenitors revealed that maturation had supported the induction of several late-stage melanocyte markers, including oculocutaneous albinism II (*OCA2*), tyrosinase (*TYR*), and melan-A (*MLANA*), whereas NC markers such as *TFAP2C*, *EDNRA*, and *EDN1* had been downregulated (Figure 5F).

Electron microscopy (EM) of human ESC-derived melanocytes (ESC-melanocytes) revealed the presence of numerous pigmented melanosomes, representing all four stages of melanosome maturation (Figure 5G). In primary skin, melanocytes reside at the basement membrane at the interface of the epidermal and dermal layers. In an organotypic skin reconstruct assay in which melanocytes and keratinocytes were seeded onto a preformed layer of fibroblasts and collagen, ESC-melanocytes phenocopied the localization of primary control melanocytes and correctly homed to the basement membrane (Figure 5H). The gene-expression profiles of ESC-melanocytes were more similar to adult than neonatal primary melanocytes (Figure S6), although ESC-melanocytes differed from both populations in their lack of Hox gene expression. It is possible that patterning conditions for BE-derived melanocytes specify a more anterior population of melanocytes as compared with primary cells isolated from posterior regions such as breast, abdominal, and foreskin tissues. However, caudal melanocytes expressing HoxB2 and HoxB4 could be established from precursors treated with RA during the early stages of differentiation (Figure S6). ESC-derived melanocytes also uniquely upregulated genes associated with protein localization and transport (Figure S6), perhaps reflecting the increased melanin production observed in comparison with primary melanocytes.
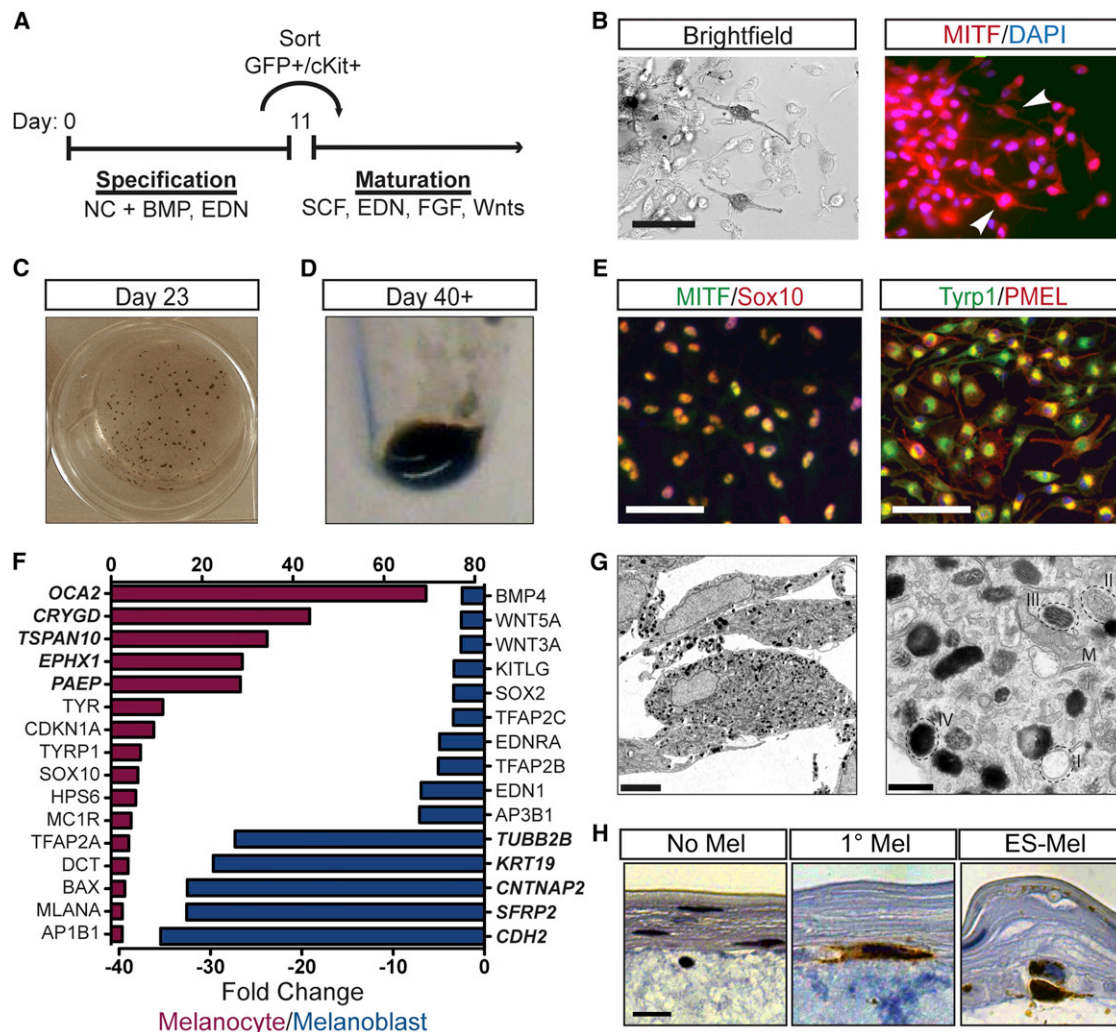
Figure 5. hESC-Derived Melanoblasts Can Be Matured to a Functional Pigmented State

(A) BE-derived melanocyte progenitors can be matured to a pigmented state following culture in media containing SCF, EDN3, FGF2, BMP, cAMP, and WNT signaling factors.

(B) Pigmented cells expressing MITF can be observed as early as 1 week after passaging. Scale bar represents 20 μm.

(C and D) Cells become progressively more pigmented, with macroscopic pigmented clusters discernible in tissue culture wells within 3 weeks (C) and cell pellets of 1 × 10^6 cells taking on a darkly pigmented phenotype (D).

(E) Extended culture supports the propagation of nearly pure populations of mature melanocytes expressing the transcription factors SOX10 and MITF, and melanosomal markers TYRP1 and PMEL. Scale bar represents 50 μm.

(F) Mature melanocytes exhibit elevated levels of mature marker expression (red) and downregulation of NC- and SC-associated markers (blue) compared with melanocyte progenitors in gene-expression analyses. Bold genes represent the top five most differentially regulated genes.

(G) Numerous pigmented melanosomes, representing all four stages of melanosome maturation (stages I–IV), are visible in the cytoplasm of ESC-derived melanocytes by EM. Scale bar represents 5 μm (left) and 500 nm (right).

(H) Tyrosinase-positive (IHC brown) ESC-derived melanocytes home to the basement membrane in organotypic artificial skin reconstructs. Scale bar represents 5 μm. Left: no melanocyte negative control; middle: primary melanocytes; right: ESC-melanocytes.

See also Figure S6.

Temporal analysis of *Sox10::GFP* and KIT expression during NC induction showed that *Sox10::GFP*-expressing cells could be detected by day 6 of differentiation (Figure 1D), whereas *Sox10::GFP*, c-kit coexpressing cells did not emerge before day 10 (Figure S4). To test the competency of Sox10-positive cells to give rise to c-kit+ melanoblasts, we isolated *Sox10::GFP* and KIT single-positive cells (GFP+/cKit− and GFP−/cKit+,

respectively), as well as double-positive and double-negative cells, by flow cytometry and replated each in maturation media. The cells were again assayed for *Sox10::GFP* and c-kit expression after 5 and 12 days. As predicted, GFP+/cKit− cells gave rise to GFP+/cKit+ and GFP−/cKit+ progeny, while GFP− cells lacked this plasticity (Figure S5). More importantly, the GFP+/cKit− and GFP−/cKit+ populations eventually differentiated

into MITF-expressing pigmented cells (Figure S5), although GFP+/cKit− cells did so with delayed kinetics. Meanwhile, the GFP−/cKit− population never gave rise to pigmented cells and could not be propagated in our maturation media. These data illustrate that, even without sorting for SOX10 or KIT, BE-treated cells can efficiently generate melanocytes under our defined maturation conditions, which will greatly facilitate studies in hESCs lacking a SOX10 reporter or in disease-specific iPSCs.

Modeling Melanosome Formation and Trafficking Defects Using iPSC-Derived Melanocytes

We next determined whether iPSC-derived melanocytes could be used to model genetic pigmentation defects. We selected two subgroups of patients with diseases involving defects in melanosome vesicle formation and trafficking: Hermansky-Pudlak syndrome (HP) and Chediak-Higashi syndrome (CH). HP encompasses eight autosomal-recessive disorders defined by deficiencies in the biogenesis of lysosome-related organelles, including melanosomes (Oh et al., 1996; Wei, 2006; Figure 6A). Patients present with a range of symptoms, including oculocutaneous albinism, platelet storage disease, and, depending on the disease subtype, immune deficiency and pulmonary fibrosis. One of the patients used in this study had a mutation in the HPS1 gene (HP1), and the other patient was deficient in AP3B1 (HP2; Figure S7). CH is caused by a mutation in the lysosomal trafficking regulator (LYST) gene that results in the persistence of abnormally large lysosome-related organelles (Karim et al., 1997; Nagle et al., 1996; Figure S7). Due to their enlarged size, melanosomes in CH patients cannot be efficiently transferred to neighboring keratinocytes, which leads to hypopigmentation (Introne et al., 1999; Figure 6A).

We established three independent iPSC lines from each patient and two control fibroblast donors using a single polycistronic lentiviral vector expressing Oct4, Klf4, Sox2, and c-Myc (Papapetrou et al., 2011; Table S2). The resulting iPSCs exhibited an hESC-like morphology and expressed the pluripotent transcription factors Oct4 and Nanog as well as the cell-surface markers Tra-1-60, SSEA3, and SSEA4 (Figure S7). Mature melanocytes expressing PMEL, SOX10, TYRP1, and MITF were derived at comparable efficiencies from each of the patient and control iPSC clones using the BE differentiation protocol (Figures 6B and S7), further illustrating the robustness of our differentiation protocol. Due to the selective growth of melanocytes in our maturation media, it was not necessary to select cells for KIT or SOX10 expression at the melanoblast stage to obtain essentially pure populations of iPSC-derived melanocytes (Figure S5). All of the HP2 iPSC-derived melanocytes exhibited a near-complete loss of pigmentation both at the macroscopic level and when quantified after cell lysis, whereas the HP1 melanocytes exhibited a more subtle phenotype that was detectable only after quantification (Figures 6C and 6D). CH melanocytes exhibited pigmentation levels lower than those observed with an African American control (control 1) but comparable to those observed with a Caucasian control (control 2; Figures 6C and 6E), which is compatible with the hypothesis that CH affects melanosome transfer rather than production. Differences in pigmentation could also be assayed by FACS analysis, with higher levels of pigmentation correlating to higher
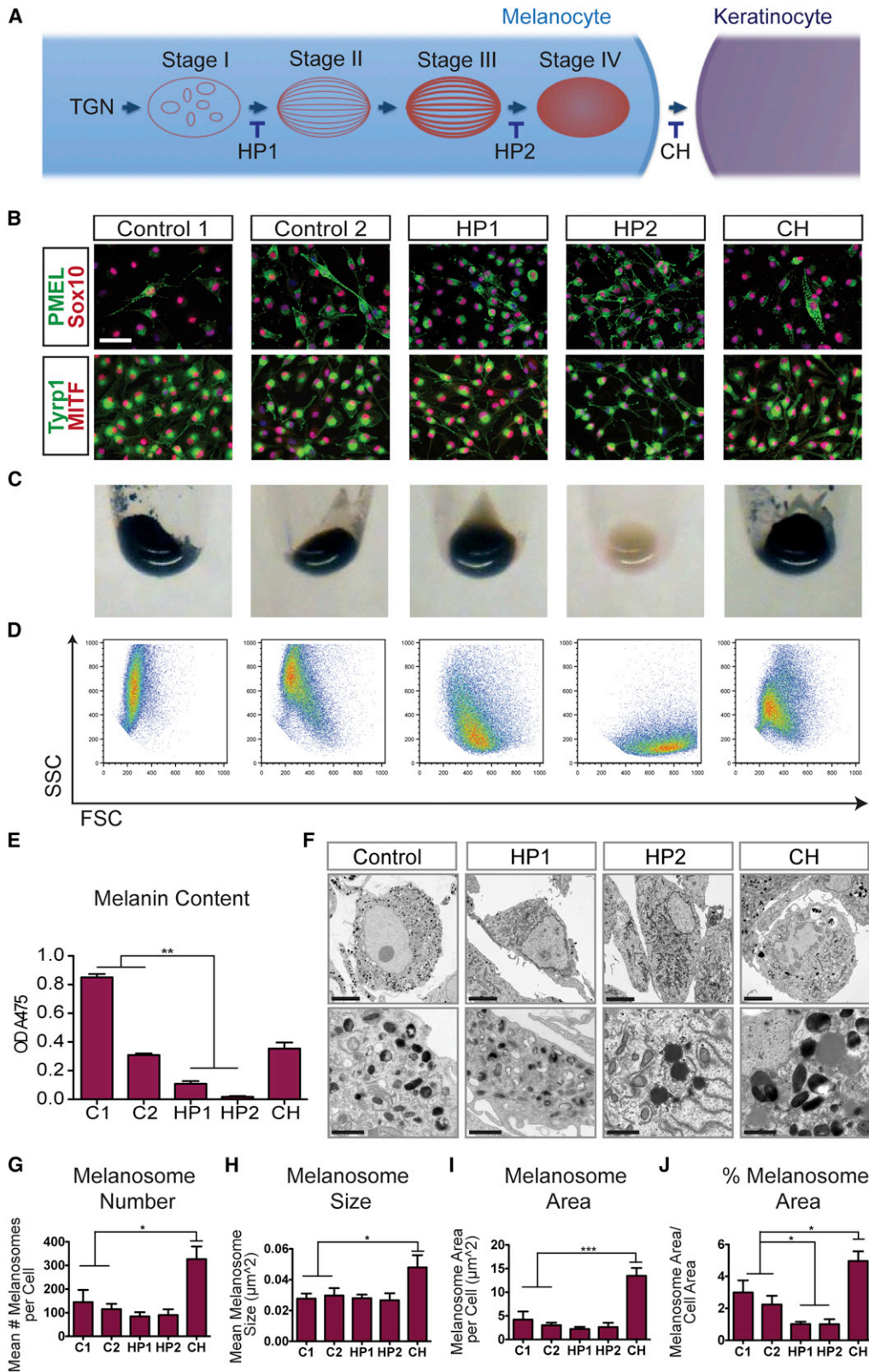
side scatter (SSC) values (Figures 6D and S7). All disease-related phenotypes were consistent among melanocytes derived from each of three independently derived iPSC clones, indicating that disease behavior reflects genome-specific differences rather than iPSC clonal variability.

The nature of the individual pigmentation defects was further analyzed at the EM level, with HP1- and HP2-derived melanocytes exhibiting a notable reduction in mature melanosomes (Figure 6F) as quantified by computer-assisted image analysis (Figures 6G–6J). There was a significant decrease in the ratio of melanosome to total cell area when compared with both the C1 and C2 controls (Figures 6F and 6J). At higher magnification, numerous dark punctae that may correspond to free melanin in the cytoplasm were also discernible in HP2 cells (Figure 6F). In contrast, CH melanocytes exhibited the most striking phenotype, with significant increases in both melanosome number and size (Figures 6G–6J). Increased melanosome number and size was further corroborated by immunofluorescence staining for the early melanosomal marker PMEL (Figure 6B). High-magnification EM analysis revealed that the CH-derived melanocytes exhibited mature but strikingly enlarged melanosomes that were not seen in the melanocytes derived from any of the other disease or control lines (Figure 6F). Global gene-expression analyses in which control- and disease-derived melanocytes were compared revealed few differences at the transcript level (Figure S7). This likely reflects the biological nature of these diseases, in which downstream processes are disrupted with little opportunity for transcriptional feedback. These data also again highlight the robust nature of our differentiation protocol in which clones derived independently from control and disease lines clustered together with high degrees of similarity.

Taken together, our data establish the derivation of melanocytes from hPSCs as a robust protocol for studying lineage specification of NC and melanocyte lineages, and as a platform for studying pigmentation-related disorders in patient-specific PSCs (Figure 7).

DISCUSSION

The specification of NC during mouse and chick development is dependent on both WNT and intermediate levels of BMP signaling generated by neighboring nonneural ectoderm and mesodermal tissues (García-Castro et al., 2002; Kléber et al., 2005; LaBonne and Bronner-Fraser, 1998; Marchant et al., 1998; Patthey et al., 2008). However, the requirement for BMP signaling is preceded in *Xenopus* models by an early need for BMP inhibition to promote the robust acquisition of neural plate identity, which in turn establishes the competence to respond to subsequent NC inductive cues (LaBonne and Bronner-Fraser, 1998; Steventon et al., 2009). Although we were able to confirm a similar requirement for early BMP inhibition in the induction of human NC, surprisingly, we did not find that continued BMP inhibition negatively impacted NC induction, even though studies in chick and *Xenopus* embryos have implicated BMP signaling during both NC induction and maintenance (Kléber et al., 2005; Marchant et al., 1998; Selleck et al., 1998). Our data are also distinct from previous observations in

(legend on next page)

A — Disease-Specific Fibroblasts

Pigmentation Phenotypes in Disease-Specific Melanocytes
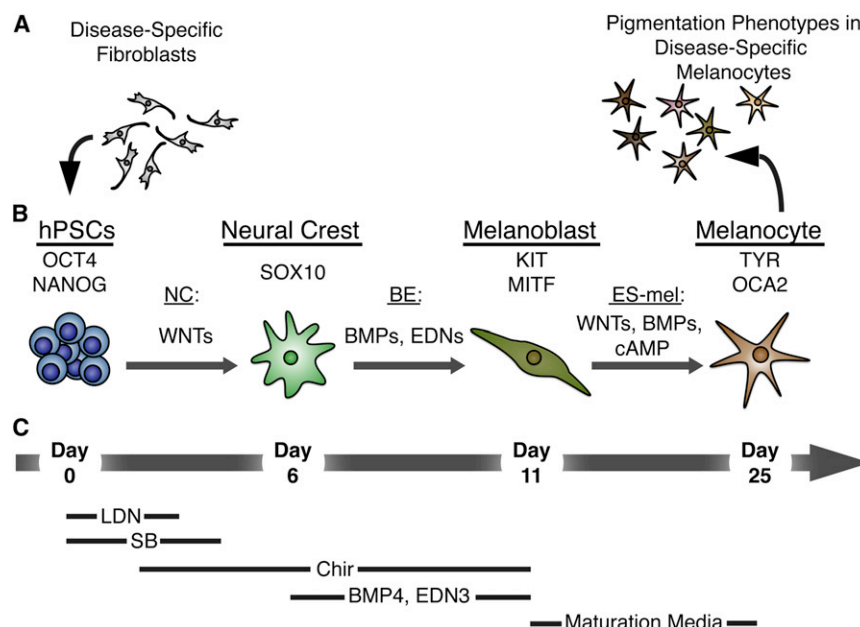
Figure 7. Disease-Specific Melanocytes that Faithfully Recapitulate Pigmentation Defects Can Be Derived from hPSCs Using a Stepwise Differentiation Paradigm

(A) Disease-specific fibroblasts from HP and CH donors were reprogrammed to establish hPSCs.

(B) Exposure of Oct4- and Nanog-expressing hPSCs to the WNT-activating NC protocol resulted in the emergence of a Sox10-positive NC population by day 6. Subsequent additional treatment with BMP4 and EDN3 (BE) skewed the specification along the melanocytic lineage to allow for the establishment of a melanoblast progenitor population expressing KIT and MITF at day 11. Further maturation under ESC-melanocyte (ESC-mel) conditions in the presence of WNTs, BMP4, and cAMP supported induction of the late melanocyte markers tyrosinase (TYR) and oculocutaneous albinism II (OCA2). Mature melanocytes were used to model the disease-specific pigmentation defects of HP and CH.

(C) Growth conditions supporting each stage of differentiation are summarized below.

p75/HNK-1-expressing NC precursors derived from hESCs via a rosette intermediate (Lee et al., 2007). Under those conditions, there was a significant decrease in the percentage of putative NC precursors following treatment with the BMP inhibitor noggin and an increase following exposure to BMP4. These discrepancies may reflect inherent differences in rosette- versus nonrosette-derived NC: the former reflects the stage of NC delamination, whereas the accelerated NC derivation conditions presented here may represent an early NC induction stage prior to the presence of a distinct neuroepithelial intermediate. Alternatively, as Sox10::GFP expression and p75/HNK-1 coexpression appear to identify overlapping but distinct NC populations, it is possible that these two subtypes of NC may exhibit different requirements for BMP signaling. It should be noted that a recent immunohistochemical study of Carnegie stage 12–18 human embryos found that HNK-1 labeled only a small subset of migrating NC cells, whereas p75 expression also broadly labeled non-NC populations (Betters et al., 2010). Future studies will be required to dissect the exact contribution of BMP pathway manipulations during hESC differentiation to NC, and to define whether differential requirements reflect distinct developmental NC stages or subtypes.

The use of Chir in our protocol offers a simple and cost-effective strategy to activate WNT signaling during NC induction. Although we were able to demonstrate robust induction of Sox10::GFP upon exposure to high doses of WNT3a (Figure S1), the concentrations of WNT3a required were cost prohibitive and not practical for routine NC induction. Chir treatment triggers rapid activation of WNT signaling pathway molecules and robust induction of a TCF::luciferase reporter (Figure S1). The critical role of WNT signaling in our NC-induction conditions is consistent with previous findings in avian systems, which demonstrated that WNT signaling is necessary and sufficient for NC induction (García-Castro et al., 2002). Similar requirements for WNT signaling to induce a p75, HNK-1 coexpressing human NC population have also been reported (Lee et al., 2007; Menendez et al., 2011); however, our study is unique in addressing the temporal requirements for WNT signaling during human NC specification. The very narrow window during which WNT signaling promoted Sox10::GFP induction was unexpected and offers a powerful tool to mechanistically define competency factors that act together with WNT in NC specification. One interesting hypothesis is that loss of competency correlates with the time course of Dkk1 induction and anterior CNS fate specification observed

Figure 6. iPSC-Derived Melanocytes Recapitulate Disease-Associated Pigmentation Defects

(A) HP and CH are disorders with defects in melanosome biogenesis and trafficking amenable for iPSC-based disease modeling.

(B) Melanocytes derived from patient-specific and control (C1 and C2) iPSCs express melanocyte-associated transcription factors and melanosomal proteins. Scale bar represents 50 μm.

(C) Cell pellets of HP2-derived melanocytes exhibit a near lack of pigmentation, whereas HP1-derived melanocytes exhibit a more subtle defect.

(D) Pigmentation levels of patient-specific melanocytes are correlated to granularity (SSC) in flow-cytometric analysis.

(E) Melanin content was determined from the absorbance of cell lysates at 475 nm.

(F) HP1- and HP2-associated pigmentation defects can be observed in electron micrographs, and CH-derived melanocytes exhibit disease-typical enlarged melanosomes. Scale bars represent 5 μm (top row) and 1 μm (bottom row).

(G–J) Stereological quantification of melanosome phenotype observed in electron micrographs.

Error bars represent the SEM from melanocytes derived from three independent iPSC lines for each disease (two lines were derived from donor C2). See also Figure S7.

during DSi (Fasano et al., 2010). This is supported by our own observation that the negative WNT regulator *SIX3* continued to be expressed when Chir treatment was not initiated until day 4. It is tempting to speculate that knockdown of *SIX3* may restore NC competence to cells at this late time point. Furthermore, it was recently reported that sequential activation of WNT signaling in the mouse embryo affects NC lineage specification, particularly along sensory neuronal and melanocyte lineages (Hari et al., 2012). It will be interesting to define whether *SOX10::GFP* NC cells induced following a Chir pulse treatment are functionally distinct from those generated upon long-term Chir treatment, particularly under conditions in which endogenous WNT signaling is further suppressed by treatment with XAV.

Our study also establishes a readily scalable, defined protocol that generates pure populations of mature melanocyte with great efficiency. Our cells recapitulate all of the structural features of wild-type melanocytes, making them suitable for a wide range of applications and future studies. In particular, the remarkable fidelity of our cells in capturing the different levels of pigmentation in Caucasian- and African-American-derived melanocytes highlights the potential utility of these cells in other fields, such as the cosmetics industry. Furthermore, this protocol allows for the stage-specific isolation of melanocyte progenitors and mature melanocytes. This will be of particular interest in studies investigating melanocyte development and malignant transformation. We also demonstrate that the axial levels of NC and melanocyte precursor populations can be readily patterned using caudalizing FGF and RA cues. The ability to derive Hox-positive versus Hox-negative human NC cells is particularly intriguing because it will enable studies of the unique plasticity reported for Hox-negative NC in the avian system (Le Douarin et al., 2004).

A recent study also identified Schwann cell precursors as an additional source of melanocytes (Adameyko et al., 2009), and EDN3 has been shown to induce the reversion of melanocytes to a bipotent progenitor (Dupin et al., 2000). It will be interesting to further explore this close association between glial and melanocyte fates, although the reported expression of Schwann-cell-associated markers in murine melanoblasts (Colombo et al., 2012) highlights the need for a thorough and careful analysis to differentiate between the origin of melanocytes from a bipotent glial-melanocyte progenitor and the derivation of melanocytes from Schwann cell precursors.

The derivation of PSCs from human fibroblasts (Park et al., 2008a; Takahashi et al., 2007; Yu et al., 2007) has been successfully applied to model human diseases (Dimos et al., 2008; Ebert et al., 2009; Park et al., 2008b), including disorders of the NC such as familial dysautonomia (Lee et al., 2009). In this study, we present an example of the modeling of melanocyte-associated disorders through derivation of patient-specific iPSCs from three distinct genetic syndromes. In each case, we were able to successfully generate patient-specific melanocytes and define pigmentation defects characteristic of each disorder in vitro. Previous iPSC-based disease modeling studies suffered greatly from variability observed between iPSC lines. Therefore, the unusual degree of fidelity we observed between melanocyte clones derived from multiple iPSC lines illustrates the highly robust nature of our melanocyte induction protocol. This estab-

lishes a framework for high-throughput screening studies to further explore disease biology or to identify novel candidate drugs affecting melanocyte specification or levels of pigmentation. A particularly attractive future strategy would be to use disease-specific melanocytes to identify drugs that can reverse easily screened pigmentation defects associated with HP1 as a surrogate assay for compounds that might also correct lysosomal function in other disease-relevant cell types, such as pulmonary pneumocytes.

Our study offers insights into the precise signaling requirements for early NC induction, melanocyte lineage specification, and melanocyte maturation. These insights can now be harnessed to establish unlimited numbers of melanocytes suitable for a broad range of applications, including a model system for the study of melanocyte pathologies and malignant melanoma origination.

EXPERIMENTAL PROCEDURES

NC and Melanocyte Differentiation
Neural induction using the DSi protocol was performed as previously described (Chambers et al., 2009, 2011; Lee et al., 2010). Briefly, dissociated hESCs and iPSCs were plated on matrigel at a density of 18,000–25,000 cells/cm^2 in MEF-conditioned hESC medium containing 10 ng/ml FGF2 and 10 μM ROCK-inhibitor (Y-27632). Cells were allowed to reach 70%–80% confluence over 3 days. Differentiation was initiated by switching to medium that included knockout serum replacement medium with 500 nM LDN193189 (Stemgent) and 10 μM SB431542 (Tocris). Beginning at day 4, the knockout serum replacement medium was gradually replaced with increasing amounts of N2 medium. For NC differentiation, the DSi protocol was adapted by treating with 3 μM CHIR99021 (Stemgent) beginning on day 2 and withdrawing LDN193189 and SB431542 at days 3 and 4, respectively. BE-derived cells were additionally treated with 25 ng/ml BMP4 and 100 nM EDN3 beginning at day 6 of differentiation. Cells were collected on day 11 for analysis or passaging.

Melanocyte Maturation and Maintenance
Day 11 dissociated BE-derived cells were replated on poly-ornithine, laminin, and fibronectin-coated plates in Neurobasal (NB; Invitrogen)/Mel medium. The NB/Mel medium was prepared by replacing the WNT3A-CM component in Mel-1 medium (Fang et al., 2006) with NB medium containing 2% B27 supplement (Invitrogen), 3 μM Chir, 25 ng/ml BMP4, and 500 μM dbcAMP. Cells were fed every other day and passaged weekly for maintenance and expansion.

Pigmentation Quantification
Melanin content was quantified by previously described methods (Friedmann and Gilchrest, 1987; Wen-Jun et al., 2008). Briefly, 2.5 × 10^5 melanocytes were collected and pelleted at 16,000 × *g* for 30 s. Cells were washed twice with PBS and then dissolved in 250 μl 1M NaOH for 40 min at 37°C. Then 100 μl of cell lysate was transferred in duplicate to 96-well plates and the OD$_{475}$ was measured with a PerkinElmer EnSpire plate reader.

Organotypic Skin Reconstruct
Organotypic skin reconstructs were established as previously described (Meier et al., 2000). Briefly, an artificial dermal layer was established by seeding human dermal fibroblasts (Invitrogen) in collagen in transwell permeable supports (Corning). After several days, human epidermal keratinocytes and primary (control) or ESC-derived melanocytes were introduced on top of the dermal layer and allowed to expand and stratify at the air-liquid interphase for an additional 2 weeks. Skin reconstructs were collected, fixed in 10% formalin, and embedded in paraffin for sectioning and immunohistochemical processing.

For further details regarding the materials and methods used in this work, see Extended Experimental Procedures.

ACCESSION NUMBERS

The gene-expression data are available in the Gene Expression Omnibus under accession number GSE45227.

SUPPLEMENTAL INFORMATION

Supplemental Information includes Extended Experimental Procedures, seven figures, and two tables and can be found with this article online at http://dx.doi.org/10.1016/j.celrep.2013.03.025.

LICENSING INFORMATION

ACKNOWLEDGMENTS

REFERENCES

Adameyko, I., Lallemend, F., Aquino, J.B., Pereira, J.A., Topilko, P., Müller, T., Fritz, N., Beljajeva, A., Mochii, M., Liste, I., et al. (2009). Schwann cell precursors from nerve innervation are a cellular origin of melanocytes in skin. Cell 139, 366–379.

Baynash, A.G., Hosoda, K., Giaid, A., Richardson, J.A., Emoto, N., Hammer, R.E., and Yanagisawa, M. (1994). Interaction of endothelin-3 with endothelin-B receptor is essential for development of epidermal melanocytes and enteric neurons. Cell 79, 1277–1285.

Betters, E., Liu, Y., Kjaeldgaard, A., Sundström, E., and García-Castro, M.I. (2010). Analysis of early human neural crest development. Dev. Biol. 344, 578–592.

Braun, M.M., Etheridge, A., Bernard, A., Robertson, C.P., and Roelink, H. (2003). Wnt signaling is required at distinct stages of development for the induction of the posterior forebrain. Development 130, 5579–5587.

Chambers, S.M., Fasano, C.A., Papapetrou, E.P., Tomishima, M., Sadelain, M., and Studer, L. (2009). Highly efficient neural conversion of human ES and iPS cells by dual inhibition of SMAD signaling. Nat. Biotechnol. 27, 275–280.

Chambers, S.M., Mica, Y., Studer, L., and Tomishima, M.J. (2011). Converting human pluripotent stem cells to neural tissue and neurons to model neurodegeneration. Methods Mol. Biol. 793, 87–97.

Chambers, S.M., Qi, Y., Mica, Y., Lee, G., Zhang, X.-J., Niu, L., Bilsland, J., Cao, L., Stevens, E., Whiting, P., et al. (2012). Combined small-molecule inhibition accelerates developmental timing and converts human pluripotent stem cells into nociceptors. Nat. Biotechnol. 30, 715–720.

Colombo, S., Champeval, D., Rambow, F., and Larue, L. (2012). Transcriptomic analysis of mouse embryonic skin cells reveals previously unreported genes expressed in melanoblasts. J. Invest. Dermatol. 132, 170–178.

Creuzet, S., Couly, G., and Le Douarin, N.M. (2005). Patterning the neural crest derivatives during development of the vertebrate head: insights from avian studies. J. Anat. 207, 447–459.

Dimos, J.T., Rodolfa, K.T., Niakan, K.K., Weisenthal, L.M., Mitsumoto, H., Chung, W., Croft, G.F., Saphier, G., Leibel, R., Goland, R., et al. (2008). Induced pluripotent stem cells generated from patients with ALS can be differentiated into motor neurons. Science 321, 1218–1221.

Dupin, E., and Le Douarin, N.M. (2003). Development of melanocyte precursors from the vertebrate neural crest. Oncogene 22, 3016–3023.

Dupin, E., Glavieux, C., Vaigot, P., and Le Douarin, N.M. (2000). Endothelin 3 induces the reversion of melanocytes to glia through a neural crest-derived glial-melanocytic progenitor. Proc. Natl. Acad. Sci. USA 97, 7882–7887.

Ebert, A.D., Yu, J., Rose, F.F., Jr., Mattis, V.B., Lorson, C.L., Thomson, J.A., and Svendsen, C.N. (2009). Induced pluripotent stem cells from a spinal muscular atrophy patient. Nature 457, 277–280.

Elkabetz, Y., Panagiotakos, G., Al Shamy, G., Socci, N.D., Tabar, V., and Studer, L. (2008). Human ES cell-derived neural rosettes reveal a functionally distinct early neural stem cell stage. Genes Dev. 22, 152–165.

Fang, D., Leishear, K., Nguyen, T.K., Finko, R., Cai, K., Fukunaga, M., Li, L., Brafford, P.A., Kulp, A.N., Xu, X., et al. (2006). Defining the conditions for the generation of melanocytes from human embryonic stem cells. Stem Cells 24, 1668–1677.

Fasano, C.A., Chambers, S.M., Lee, G., Tomishima, M.J., and Studer, L. (2010). Efficient derivation of functional floor plate tissue from human embryonic stem cells. Cell Stem Cell 6, 336–347.

Friedmann, P.S., and Gilchrest, B.A. (1987). Ultraviolet radiation directly induces pigment production by cultured human melanocytes. J. Cell. Physiol. 133, 88–94.

Fujimura, N., Vacik, T., Machon, O., Vlcek, C., Scalabrin, S., Speth, M., Diep, D., Krauss, S., and Kozmik, Z. (2007). Wnt-mediated down-regulation of Sp1 target genes by a transcriptional repressor Sp5. J. Biol. Chem. 282, 1225–1237.

García-Castro, M.I., Marcelle, C., and Bronner-Fraser, M. (2002). Ectodermal Wnt function as a neural crest inducer. Science 297, 848–851.

Hari, L., Miescher, I., Shakhova, O., Suter, U., Chin, L., Taketo, M., Richardson, W.D., Kessaris, N., and Sommer, L. (2012). Temporal control of neural crest lineage generation by Wnt/β-catenin signaling. Development 139, 2107–2117.

Huizing, M., Scher, C.D., Strovel, E., Fitzpatrick, D.L., Hartnell, L.M., Anikster, Y., and Gahl, W.A. (2002). Nonsense mutations in ADTB3A cause complete deficiency of the beta3A subunit of adaptor complex-3 and severe Hermansky-Pudlak syndrome type 2. Pediatr. Res. 51, 150–158.

Introne, W., Boissy, R.E., and Gahl, W.A. (1999). Clinical, molecular, and cell biological aspects of Chediak-Higashi syndrome. Mol. Genet. Metab. 68, 283–303.

Karim, M.A., Nagle, D.L., Kandil, H.H., Bürger, J., Moore, K.J., and Spritz, R.A. (1997). Mutations in the Chediak-Higashi syndrome gene (CHS1) indicate requirement for the complete 3801 amino acid CHS protein. Hum. Mol. Genet. 6, 1087–1089.

Kléber, M., Lee, H.-Y., Wurdak, H., Buchstaller, J., Riccomagno, M.M., Ittner, L.M., Suter, U., Epstein, D.J., and Sommer, L. (2005). Neural crest stem cell maintenance by combinatorial Wnt and BMP signaling. J. Cell Biol. 169, 309–320.

Kriks, S., Shim, J.-W., Piao, J., Ganat, Y.M., Wakeman, D.R., Xie, Z., Carrillo-Reid, L., Auyeung, G., Antonacci, C., Buch, A., et al. (2011). Dopamine neurons derived from human ES cells efficiently engraft in animal models of Parkinson's disease. Nature 480, 547–551.

Kunisada, T., Yoshida, H., Yamazaki, H., Miyamoto, A., Hemmi, H., Nishimura, E., Shultz, L.D., Nishikawa, S., and Hayashi, S. (1998). Transgene expression of steel factor in the basal layer of epidermis promotes survival, proliferation, differentiation and migration of melanocyte precursors. Development 125, 2915–2923.

LaBonne, C., and Bronner-Fraser, M. (1998). Neural crest induction in Xenopus: evidence for a two-signal model. Development 125, 2403–2414.

Lagutin, O.V., Zhu, C.C., Kobayashi, D., Topczewski, J., Shimamura, K., Puelles, L., Russell, H.R.C., McKinnon, P.J., Solnica-Krezel, L., and Oliver, G. (2003). Six3 repression of Wnt signaling in the anterior neuroectoderm is essential for vertebrate forebrain development. Genes Dev. 17, 368–379.

Lahav, R., Ziller, C., Dupin, E., and Le Douarin, N.M. (1996). Endothelin 3 promotes neural crest cell proliferation and mediates a vast increase in melanocyte number in culture. Proc. Natl. Acad. Sci. USA 93, 3892–3897.

Lavado, A., Lagutin, O.V., and Oliver, G. (2008). Six3 inactivation causes progressive caudalization and aberrant patterning of the mammalian diencephalon. Development 135, 441–450.

Le Douarin, N.M., Creuzet, S., Couly, G., and Dupin, E. (2004). Neural crest cell plasticity and its limits. Development 131, 4637–4650.

Lee, G., Kim, H., Elkabetz, Y., Al Shamy, G., Panagiotakos, G., Barberi, T., Tabar, V., and Studer, L. (2007). Isolation and directed differentiation of neural crest stem cells derived from human embryonic stem cells. Nat. Biotechnol. 25, 1468–1475.

Lee, G., Papapetrou, E.P., Kim, H., Chambers, S.M., Tomishima, M.J., Fasano, C.A., Ganat, Y.M., Menon, J., Shimizu, F., Viale, A., et al. (2009). Modelling pathogenesis and treatment of familial dysautonomia using patient-specific iPSCs. Nature 461, 402–406.

Lee, G., Chambers, S.M., Tomishima, M.J., and Studer, L. (2010). Derivation of neural crest cells from human pluripotent stem cells. Nat. Protoc. 5, 688–701.

Luo, R., Gao, J., Wehrle-Haller, B., and Henion, P.D. (2003). Molecular identification of distinct neurogenic and melanogenic neural crest sublineages. Development 130, 321–330.

Marchant, L., Linker, C., Ruiz, P., Guerrero, N., and Mayor, R. (1998). The inductive properties of mesoderm suggest that the neural crest cells are specified by a BMP gradient. Dev. Biol. 198, 319–329.

Meier, F., Nesbit, M., Hsu, M.Y., Martin, B., Van Belle, P., Elder, D.E., Schaumburg-Lever, G., Garbe, C., Walz, T.M., Donatien, P., et al. (2000). Human melanoma progression in skin reconstructs : biological significance of bFGF. Am. J. Pathol. 156, 193–200.

Meijer, L., Flajolet, M., and Greengard, P. (2004). Pharmacological inhibitors of glycogen synthase kinase 3. Trends Pharmacol. Sci. 25, 471–480.

Menendez, L., Yatskievych, T.A., Antin, P.B., and Dalton, S. (2011). Wnt signaling and a Smad pathway blockade direct the differentiation of human pluripotent stem cells to multipotent neural crest cells. Proc. Natl. Acad. Sci. USA 108, 19240–19245.

Nagle, D.L., Karim, M.A., Woolf, E.A., Holmgren, L., Bork, P., Misumi, D.J., McGrail, S.H., Dussault, B.J., Jr., Perou, C.M., Boissy, R.E., et al. (1996). Identification and mutation analysis of the complete gene for Chediak-Higashi syndrome. Nat. Genet. 14, 307–311.

Nissan, X., Larribere, L., Saidani, M., Hurbain, I., Delevoye, C., Feteira, J., Lemaitre, G., Peschanski, M., and Baldeschi, C. (2011). Functional melanocytes derived from human pluripotent stem cells engraft into pluristratified epidermis. Proc. Natl. Acad. Sci. USA 108, 14861–14866.

Oh, J., Bailin, T., Fukai, K., Feng, G.H., Ho, L., Mao, J.I., Frenk, E., Tamura, N., and Spritz, R.A. (1996). Positional cloning of a gene for Hermansky-Pudlak syndrome, a disorder of cytoplasmic organelles. Nat. Genet. 14, 300–306.

Papapetrou, E.P., Lee, G., Malani, N., Setty, M., Riviere, I., Tirunagari, L.M.S., Kadota, K., Roth, S.L., Giardina, P., Viale, A., et al. (2011). Genomic safe harbors permit high β-globin transgene expression in thalassemia induced pluripotent stem cells. Nat. Biotechnol. 29, 73–78.

Park, I.-H., Zhao, R., West, J.A., Yabuuchi, A., Huo, H., Ince, T.A., Lerou, P.H., Lensch, M.W., and Daley, G.Q. (2008a). Reprogramming of human somatic cells to pluripotency with defined factors. Nature 451, 141–146.

Park, I.H., Arora, N., Huo, H., Maherali, N., Ahfeldt, T., Shimamura, A., Lensch, M.W., Cowan, C., Hochedlinger, K., and Daley, G.Q. (2008b). Disease-specific induced pluripotent stem cells. Cell 134, 877–886.

Patthey, C., Gunhaga, L., and Edlund, T. (2008). Early development of the central and peripheral nervous systems is coordinated by Wnt and BMP signals. PLoS One 3, e1625.

Reid, K., Nishikawa, S., Bartlett, P.F., and Murphy, M. (1995). Steel factor directs melanocyte development in vitro through selective regulation of the number of c-kit+ progenitors. Dev. Biol. 169, 568–579.

Reid, K., Turnley, A.M., Maxwell, G.D., Kurihara, Y., Kurihara, H., Bartlett, P.F., and Murphy, M. (1996). Multiple roles for endothelin in melanocyte development: regulation of progenitor number and stimulation of differentiation. Development 122, 3911–3919.

Ring, D.B., Johnson, K.W., Henriksen, E.J., Nuss, J.M., Goff, D., Kinnick, T.R., Ma, S.T., Reeder, J.W., Samuels, I., Slabiak, T., et al. (2003). Selective glycogen synthase kinase 3 inhibitors potentiate insulin activation of glucose transport and utilization in vitro and in vivo. Diabetes 52, 588–595.

Selleck, M.A., García-Castro, M.I., Artinger, K.B., and Bronner-Fraser, M. (1998). Effects of Shh and Noggin on neural crest formation demonstrate that BMP is required in the neural tube but not ectoderm. Development 125, 4919–4930.

Steel, K.P., Davidson, D.R., and Jackson, I.J. (1992). TRP-2/DT, a new early melanoblast marker, shows that steel growth factor (c-kit ligand) is a survival factor. Development 115, 1111–1119.

Steventon, B., Araya, C., Linker, C., Kuriyama, S., and Mayor, R. (2009). Differential requirements of BMP and Wnt signalling during gastrulation and neurulation define two steps in neural crest induction. Development 136, 771–779.

Takahashi, K., Tanabe, K., Ohnuki, M., Narita, M., Ichisaka, T., Tomoda, K., and Yamanaka, S. (2007). Induction of pluripotent stem cells from adult human fibroblasts by defined factors. Cell 131, 861–872.

Thomas, A.J., and Erickson, C.A. (2008). The making of a melanocyte: the specification of melanoblasts from the neural crest. Pigment Cell Melanoma Res. 21, 598–610.

Veeman, M.T., Slusarski, D.C., Kaykas, A., Louie, S.H., and Moon, R.T. (2003). Zebrafish prickle, a modulator of noncanonical Wnt/Fz signaling, regulates gastrulation movements. Curr. Biol. 13, 680–685.

Wei, M.L. (2006). Hermansky-Pudlak syndrome: a disease of protein trafficking and organelle function. Pigment Cell Res. 19, 19–42.

Weidinger, G., Thorpe, C.J., Wuennenberg-Stapleton, K., Ngai, J., and Moon, R.T. (2005). The Sp1-related transcription factors sp5 and sp5-like act downstream of Wnt/beta-catenin signaling in mesoderm and neuroectoderm patterning. Curr. Biol. 15, 489–500.

Wen-Jun, L., Hai-Yan, W., Wei, L., Ke-Yu, W., and Rui-Ming, W. (2008). Evidence that geniposide abrogates norepinephrine-induced hypopigmentation by the activation of GLP-1R-dependent c-kit receptor signaling in melanocyte. J. Ethnopharmacol. 118, 154–158.

Xu, J., Lamouille, S., and Derynck, R. (2009). TGF-beta-induced epithelial to mesenchymal transition. Cell Res. 19, 156–172.

Yamane, T., Hayashi, S., Mizoguchi, M., Yamazaki, H., and Kunisada, T. (1999). Derivation of melanocytes from embryonic stem cells in culture. Dev. Dyn. 216, 450–458.

Yoshida, H., Kunisada, T., Kusakabe, M., Nishikawa, S., and Nishikawa, S.I. (1996). Distinct stages of melanocyte differentiation revealed by anlaysis of nonuniform pigmentation patterns. Development 122, 1207–1214.

Yu, J., Vodyanik, M.A., Smuga-Otto, K., Antosiewicz-Bourget, J., Frane, J.L., Tian, S., Nie, J., Jonsdottir, G.A., Ruotti, V., Stewart, R., et al. (2007). Induced pluripotent stem cell lines derived from human somatic cells. Science 318, 1917–1920.